Mechanics of Materials 133 (2019) 138–153

Contents lists available at ScienceDirect

Mechanics of Materials

journal homepage: www.elsevier.com/locate/mechmat

Advanced constitutive model for repeated stress relaxation accounting for transient mobile dislocation density and internal stress

Anand Varma[a], Hariharan Krishnaswamy[b,*], Jayant Jain[a], Myoung-Gyu Lee[c,*], Frédéric Barlat[d]

[a] Department of Material Science and Engineering, Indian Institute of Technology Delhi, New Delhi 110016, India
[b] Mechanical Engineering, Indian Institute of Technology Madras, Chennai 600036, India
[c] Department of Material Science and Engineering and RIAM, Seoul National University, Seoul, Republic of Korea
[d] Graduate Institute of Ferrous Technology, Pohang University of Science and Technology, Pohang, Republic of Korea

ARTICLE INFO

Keywords:
Repeated stress relaxation
Activation volume
Dislocation density model

ABSTRACT

Repeated stress relaxation tests are used to characterize the macroscopic time dependent behavior in metals. During stress relaxation, the mobile dislocation density and internal stress vary continuously with time. The phenomenological models available do not provide a comprehensive mathematical framework to account for transient effects during stress relaxation accurately. An advanced stress relaxation model based on the logarithmic model is proposed in the present work to overcome the limitations of existing models. The proposed model is found to fit the experimental data of SS 316 better than the available models. The proposed model in combination with Kocks–Mecking type dislocation density model is utilized to predict the rate of strain hardening during relaxation

1. Introduction

Stress relaxation is one of the simplest transient tests used to estimate the parameters related to thermally activated plastic deformation such as internal stress and activation volume. The flow stress (σ) applied during plastic deformation is the sum of internal (or athermal) stress, 'σ_i' and effective (or thermal) stress, 'σ^*' required to overcome the long range and short range obstacles respectively.

$$\sigma = \sigma_i + \sigma^* \tag{1}$$

A typical stress relaxation test is performed by interrupting an uniaxial tensile test for a pre-defined time interval (in the order of 60s) at a fixed total strain. The flow stress of a rate dependent metallic material drops continuously during this hold time. Since the total strain ε_{total} remains invariant during the test duration, the plastic strain rate, $\dot{\varepsilon} = \frac{-1}{E}\frac{d\sigma}{dt} = \frac{-\dot{\sigma}}{E}$. The simplification inherently assumes that there is no viscoelastic behavior during stress relaxation and is widely adopted (Mohebbi and Akbarzadeh, 2017; Wang et al., 2016b; Caillard and Martin, 2003; Krempl, 2001; Dotsenko, 1979). Although the possibility of anelasticity during relaxation has been discussed in the past (Hart, 1970; Rohde et al., 1981), the experimental inferences were not direct and did not consider the change in mobile dislocation density. Therefore, time dependent elasticity is generally ignored in stress relaxation studies (Krempl, 2001). However, viscoelasticity can influence the high temperature relaxation behavior (Sinha, 2003; Ma et al., 2018; Zheng et al., 2018) and are not considered in the present work. The rate dependent behavior during stress relaxation can be modeled using Orowan equation, $\dot{\varepsilon} = \phi\rho_m bv$, where ϕ is a constant, ρ_m is the mobile dislocation density and v is the average dislocation velocity.

Substituting $\dot{\varepsilon} = \frac{-\dot{\sigma}}{E}$ in Orowan equation,

$$\frac{d\sigma}{dt} = -E\phi\rho_m bv \tag{2}$$

which forms the basis of most of the stress relaxation models

The classical studies on stress relaxation (Gupta and Li, 1970; Dotsenko, 1979) assumed that σ_i[1] and ρ_m remain invariant during stress relaxation, perhaps based on the general understanding of strain rate jump tests which supposedly does not influence the dislocation substructure. From Eqs. (1) and (2),

$$\frac{d\sigma^*}{dt} = \frac{d\sigma}{dt} = -E\phi\rho_m bv \tag{3}$$

The assumption of constant ρ_m during relaxation suggests that the stress drop is attributed purely to the change in average dislocation

* Corresponding authors.
E-mail addresses: hariharan@iitm.ac.in (H. Krishnaswamy), jayantj@iitd.ac.in (J. Jain), myounglee@snu.ac.kr (M.-G. Lee), f.barlat@postech.ac.kr (F. Barlat).

[1] It will shown in subsequent sections that the internal stress does not remain constant during stress relaxation. However, the variation of internal stress will be proportional to σ and hence the simplification in Eq. (3) is not affected.

https://doi.org/10.1016/j.mechmat.2019.03.009
Received 29 November 2018; Received in revised form 4 March 2019
Available online 19 March 2019

velocity, v. An empirical relation of average dislocation velocity after (Johnston and Gilman, 1959) led to the power law model (Gupta and Li, 1970).

$$\sigma - \sigma_i = K(t + a)^{-n} \tag{4}$$

where $K = \{-E\phi\rho_m bB(1-m)\}^{-n}$, $n = \frac{-1}{1-m}$ and a is the integration constant.

Considering plastic deformation as a thermally activated process, the rate form of velocity ($v = v_0 \exp(\frac{-\Delta G}{kT})$), can be substituted in Orowan equation, which upon integration (Dotsenko, 1979; Caillard and Martin, 2003) led to the logarithmic model,

$$\sigma_0 - \sigma = \alpha \ ln\{1 + \beta t\} \tag{5}$$

where α and β are material constants. It can be shown that $\alpha = kT/V^*$ and $\beta = \frac{V^* E\dot{\varepsilon}_{p0}}{kT} exp(-\frac{\Delta G_0 - \sigma_0 V^* + \sigma_i V^*}{kT})$, σ_0 refers to the stress at the beginning of relaxation ($t = 0$) and V^* is the activation volume referring to the average volume swept by a moving dislocation segment during plastic deformation under a given stress state (Anderson et al., 2017). The metallurgical parameters, σ_i and V^* can be estimated by fitting the σ vs. t data during stress relaxation using the models described by Eqs. (4) and (5) (Trojanová et al., 2011; Duhamel et al., 2010; Guo et al., 2018). Although both the models have been successfully used in literature, there is no rationale on the choice of one model over the other for a given material and deformation condition.

It is evident from Orowan equation that $\partial\dot{\varepsilon}_p/\partial t = \phi b\{\rho_m \frac{\partial v}{\partial t} + v\frac{\partial \rho_m}{\partial t}\}$, thus the stress drop during stress relaxation, $\Delta\sigma$ can be modeled either by treating v or ρ_m as constant or by allowing the variation of both. The non-constancy of σ_i and ρ_m during stress relaxation were long known (Okazaki et al., 1976; Dotsenko, 1979) almost since when Eqs. (4) and (5) were proposed, but their variation was thought to be negligible. Subsequent studies involving repeated relaxation tests (Caillard and Martin, 2003; Spätig et al., 1993) and other microstructural studies (Mohebbi et al., 2015; Li, 2000; Wang et al., 2017; Varma et al., 2018) report (Fig. 1) that it is essential to consider the variation of mobile dislocation density when modeling stress relaxation. Accounting for the transient nature of σ_i irrespective of its magnitude assumes importance in various problems. For instance, when stress relaxation data is used to estimate the activation parameters of deformation (Mohebbi et al., 2015; Guo et al., 2018), even a small change in σ_i can influence the accuracy. Similarly, it has been shown (Li and Chau, 2006) that a critical value of internal stress is required to initiate fracture in metallic materials. Stress relaxation phenomenon is been utilized to increase the ductility of metallic materials (Hariharan et al., 2016; Bong et al., 2016; Hariharan et al., 2013), the mechanism of which is related to stress homogenization during relaxation (Varma et al., 2018; Majidi et al., 2016). Recently, Wang et al. (2016a, 2017) extended elasto-viscoplastic self consistent(EVPSC) model incorporating intra-granular stress distribution to predict stress relaxation. They showed that the average resolved shear stress (which can be correlated to internal stress) decreases during stress relaxation in AZ31 and SS 316LN.

Limited attempts have been made in the past to account for the variation of ρ_m and σ_i in stress relaxation model (Okazaki et al., 1976; Xiao and Bai, 1998; Caillard and Martin, 2003; Mohebbi et al., 2015; Hariharan et al., 2016). The logarithmic model modified by Caillard and Martin (2003) is widely used and shall henceforth be referred as 'model1'. The advantage of the model is that the original mathematical form of the logarithmic model remains unaltered. The effect of ρ_m and σ_i is accounted through a scaling constant, Ω defined (Caillard and Martin, 2003) as

$$\Omega V^* = V_a \tag{6}$$

where V_a is the apparent activation volume, which is different from V^* due to the change in σ_i and ρ_m.

The variation of ρ_m is expected to share a similar mathematical form of v, (Caillard and Martin, 2003; Diologent et al., 2011)

$$\frac{\rho_{m(t)}}{\rho_{m0}} = (v/v_0)^p \tag{7}$$

where p is the exponent.

Orowan equation, when combined with Eq. (7), yields $\frac{\dot{\varepsilon}}{\dot{\varepsilon}_0} = \frac{\rho_m v}{\rho_{m0} v_0} = \frac{\rho_m^{\frac{1+p}{p}}}{\rho_{m0}}$. $\because \dot{\varepsilon} = -\dot{\sigma}/E$ during stress relaxation, the logarithmic model gives $\frac{\dot{\varepsilon}}{\dot{\varepsilon}_0} = \frac{1}{1+\beta t}$. Therefore, the variation of ρ_m can be derived as Caillard and Martin (2003),

$$\frac{\rho_{m(t)}}{\rho_{m0}} = \left(\frac{1}{1+\beta t}\right)^{p/1+p} \tag{8}$$

The change in internal stress during relaxation is usually negligible and can be modeled (Dotsenko, 1979; Caillard and Martin, 2003) as a linear function of plastic strain change.

$$\Delta\sigma_{i(t)} \propto \Delta\varepsilon_p(t) = \frac{\theta_r \Delta\sigma(t)}{E} \tag{9}$$

The solution seems elegant given that the original mathematical form is preserved and only V^* is replaced with ΩV^*. However, when integrating the stress rate, β should vary with time to accommodate the change in ρ_m. Treating β as a constant and accommodating the variation of ρ_m in α is incorrect. This error restricts the slope of the model $|S| = 1$ at sufficiently large time. Experimental observations by Mohebbi et al. (2015) showed that $|S| \neq 1$. In addition to the above, the estimation of rate of hardening during relaxation, θ_r is not well defined. As a first approximation, $\theta = \frac{d\sigma}{d\varepsilon}$ obtained from monotonic tensile tests can be used. However, θ includes the effect of both σ_i and σ^* whereas θ_r is related primarily with σ_i.

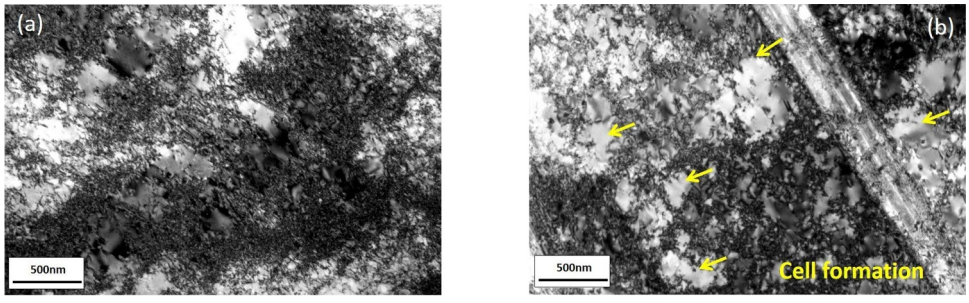

(a) (b)

Fig. 1. Bright-field TEM micrographs of the samples tested in tension at a strain rate of 10^{-2} s^{-1} at a strain of 25% with (a) unloaded at 25% strain with no relaxation and (b) unloaded after a holding period of 60 s. Note that the arrows in (b) indicate the cell formation (reproduced from Varma et al., 2018).

In the present work, it is attempted to propose a new model that can accurately represent the evolution of ρ_m and σ_i during stress relaxation.

2. New model for stress relaxation

The non-constancy of ρ_m during relaxation can be accommodated by either (i) introducing a time dependent evolution of the constant β or (ii) by incorporating an mathematical expression for the variation of ρ_m in the differential form of the model. The first approach was generalized by Mohebbi et al. (2015) and recently adopted in Hariharan et al. (2016) as given below.

$$\sigma_0 - \sigma = \bar{\alpha} \ln(1 + \bar{\beta}_0 e^{\lambda t} t) \tag{10}$$

where $\bar{\alpha}$ accounts for the variation of σ_i through Eq. (9) and λ is a fitting constant.

The above model shall be referred to as 'model2' in the rest of the manuscript. During stress relaxation, σ decrease continuously and saturates, for which the mathematical necessity is $\frac{d\sigma}{dt} \leq 0$ for all the values of t.

$$\left(\frac{d\sigma}{dt}\right)_{model2} = -\frac{\bar{\alpha} e^{\lambda t}(1 + \lambda t)}{1 + \beta_0 e^{\lambda t} t}$$

Since $\lambda < 0$ in Eq. (10), $\frac{d\sigma}{dt} > 0$ when $t > -1/\lambda$, which is not physically plausible.

In the present work, the second approach is adopted to propose a new phenomenological model for stress relaxation. The advantage of the approach is that the variation of ρ_m is introduced in the differential form of stress relaxation equation, which upon integration directly yields a mathematically consistent solution.

A general expression for $\rho_{m(t)}$ is given by

$$\frac{\rho_{m(t)}}{\rho_{m0}} = \left(\frac{A}{t + a}\right)^{\lambda}$$

where λ is a material constant.

The above equation reduces to the solution proposed by Xiao and Bai (1998) when $\lambda = 1$ and to Caillard and Martin (2003) when $A = a = \frac{1}{\beta}$ & $\lambda = \frac{p}{1 + p}$. At the initiation of stress relaxation ($t = 0$), $\rho_m = \rho_{m0}$, which simplifies to Eq. (11), irrespective of the value of the constant 'a'. The role of 'a' in the equation is to avoid singularity at $t = 0$.

$$\frac{\rho_{m(t)}}{\rho_{m0}} = \left(\frac{a}{t + a}\right)^{\lambda} \tag{11}$$

Substituting Eq. (11) & average dislocation velocity (rate form) in Eq. (3),

$$-\frac{d\sigma}{dt} = E\phi b \rho_{m0} \left(\frac{a}{t + a}\right)^{\lambda} exp\left(-\frac{\Delta G_0 - \sigma V^* + \sigma_i V^*}{kT}\right) \tag{12}$$

Upon integrating Eq. (12) (refer Section A.1), the following new model is obtained

$$\sigma_0 - \sigma = \alpha \, ln\left[1 + \bar{\beta}\left\{\left(\frac{t + a}{a}\right)^{1-\lambda} - 1\right\}\right] \tag{13}$$

where $\alpha = kT/V^*$ and $\bar{\beta} = E\phi b \rho_{m0} \frac{V^*}{kT} \frac{a}{1-\lambda} \exp\left(-\frac{\Delta G_0 - \sigma_0 * V^*}{kT}\right)$.

σ_0* refers to the effective stress at the beginning of relaxation when time, $t = 0$. $\bar{\beta}$ in Eq. (13) is distinctly different from model 2.

2.1. Modeling internal stress change

$(\sigma_i)_t$ is highly dependent on the substructure (Hu et al., 2016). During stress relaxation, the substructure is altered by the reduction of ρ_m through dislocation annihilation and strain hardening due to plastic strain ($\Delta\varepsilon_p = -\Delta\sigma/E$) (Dotsenko, 1979). It is to be clarified that annihilation in the present manuscript unless and otherwise specified, explicitly refers to the dislocation annihilation[2] during stress relaxation. In general, the change in internal stress is modeled as a linear function of plastic strain, which accounts only for strain hardening and not for dislocation annihilation (Dotsenko, 1979).

In the present work, an alternate approach to determine $\Delta\sigma_i$ is demonstrated using the dislocation density based model. The classical Kocks–Mecking–Estrin (K–M–E) model (Kocks and Mecking, 2003; Estrin, 1998) relates internal stress to total dislocation density as

$$\sigma_i = M\varphi\mu b\sqrt{\rho} \tag{14}$$

where M is the Taylor factor, φ a fitting constant, μ is the shear modulus and b denotes the Burgers vector. Using a power law kinetic equation (Estrin, 1998), rate dependent flow stress (σ) can be calculated as

$$\sigma = \sigma_i(\dot{\varepsilon}/\dot{\varepsilon}_0)^m \tag{15}$$

where $\dot{\varepsilon}_0$ and m are experimentally determined material constants. The evolution of dislocation density during strain hardening consists of a storage ($k_1\sqrt{\rho}$) and recovery term ($k_2\rho$) (Kocks and Mecking, 2003).

$$\frac{d\rho}{d\varepsilon} = M\{k_1\sqrt{\rho} - k_2\rho\} \tag{16}$$

where $k_1$andk_2 are constants.

Several modifications of dislocation density based model have been proposed (Barlat et al., 2002; Lindgren et al., 2017; Hamelin et al., 2011; Benzerga, 2008) to accommodate different deformation mechanisms such as the effect of solute concentration, temperature, strain rate (Kreyca and Kozeschnik, 2018; Babu and Lindgren, 2013; Fan and Yang, 2011; Hansen et al., 2013) and grain size (Khan and Liu, 2016; Fan and Yang, 2011; Jiang et al., 2018). The approach has also been proven to model the changes in deformation strain path (Beyerlein and Tomé, 2007; Carvalho Resende et al., 2013; Jeong et al., 2017) such as latent hardening (Zecevic and Knezevic, 2018; Bertin et al., 2014), Bauschinger effect (Rauch et al., 2007; Wang et al., 2017) and cyclic loading (Muhammad et al., 2017; Zecevic and Knezevic, 2015; Ha et al., 2017; Jeong et al., 2017).

The classical K–M–E model (Eq. (16)) used to demonstrate the evolution of internal stress during stress relaxation can be rewritten as

$$\frac{d\rho}{dt} = \frac{d\rho}{d\varepsilon}\frac{d\varepsilon}{dt} = M\{k_1\sqrt{\rho} - k_2\rho\}\dot{\varepsilon}$$

$\dot{\varepsilon}$ varies continuously during stress relaxation. From Eq. (13), $\dot{\varepsilon}$ for the proposed model is given as

$$\dot{\varepsilon} = \frac{-1}{E}\frac{d\sigma}{dt} = \psi\frac{(t + a)^{-\lambda}}{1 + \beta\left\{\left(\frac{t+a}{a}\right)^{1-\lambda} - 1\right\}} \tag{17}$$

where $\psi = \frac{\alpha\beta(1-\lambda)a^{(\lambda-1)}}{E}$. Therefore the time dependent dislocation evolution during stress relaxation is given by

$$\frac{d\rho}{dt} = M\psi\{k_1\sqrt{\rho} - k_2\rho\}\left[\frac{(t + a)^{-\lambda}}{1 + \beta\left\{\left(\frac{t+a}{a}\right)^{1-\lambda} - 1\right\}}\right] \tag{18}$$

A monotonic stress relaxation test involves pre-straining the material to say ε_0. Let the total dislocation density at ε_0 be indicated as $(\rho)_{\varepsilon_0} = \tilde{\rho}$. The time dependent evolution of ρ during stress relaxation can be conveniently written (refer Section A.2) as,

$$\rho_t = \rho_f + \rho_r \tag{19}$$

where ρ_f and ρ_r respectively indicates forward and reverse dislocation

[2] It is generally accepted that the annihilation of dislocations occur during monotonic loading without stress relaxation also. However, the net effect of dislocation multiplication and annihilation during monotonic loading is a positive increment in dislocation density with plastic strain.

densities.

The decomposition of forward and reverse dislocation is similar to the framework adopted by Rauch et al. (2007) to analyze the Bauschinger effect. This approach is justified from a perspective that the annihilation mechanism during relaxation and Bauschinger effect are similar which can be explained using the classical Orowan mechanism (Brown, 1977; Hu et al., 2016) illustrated in Section A.3. The main difference between annihilation in Bauschinger effect and stress relaxation is that the former is effected by stored potential energy (elastic energy) whereas the latter is due to the kinetic energy of the mobile dislocations.

Following the above discussion, $\sigma_i = M\alpha\mu b\sqrt{\rho_f + \rho_r}$. During monotonic loading, forward dislocations get accumulated (Eq. (18)) ($\rho_f = \rho$) whereas reverse dislocations remain null ($\rho_r = 0$). When stress relaxation begin at t_0, the mobile dislocation density decrease following Eq. (11). The reverse dislocation (ρ_r) at $t = t_0$ is considered to be a constant fraction of total dislocation density, $\Gamma\tilde{\rho}$ (Rauch et al., 2007; Hariharan et al., 2017). An additional evolutionary law (Eq. (20)) as proposed in Hariharan et al. (2017) is used to model the annihilation of ρ_r with time.

$$\frac{d\rho_r}{dt} = \frac{d\rho_r}{d\varepsilon}\frac{d\varepsilon}{dt} = -qMK_1\sqrt{\rho_f}\frac{\rho_r}{\tilde{\rho}}\dot{\varepsilon} \tag{20}$$

where q is a scalar indicating the rate of annihilation of reverse dislocations. Substituting $\dot{\varepsilon}$ from Eq. (17) in the above expression,

$$\frac{d\rho_r}{dt} = -\psi qMK_1\sqrt{\rho_f}\frac{\rho_r}{\tilde{\rho}}\left[\frac{(t+a)^{\lambda}}{1+\beta\left\{\left(\frac{t+a}{a}\right)^{1-\lambda}-1\right\}}\right] \tag{21}$$

The remaining dislocations ($\rho_f = (1-\Gamma)\tilde{\rho}$) continue to evolve following Eq. (18).

The parameters of dislocation density model for SS 316 (Table 1) considered in the present work is estimated by curve fitting the stress-strain curve at room temperature and a strain rate of $1e^{-2}s^{-1}$. The material constants, M, μ and b are chosen from literature (Rauch et al., 2007). The predicted stress strain curve compares well with the experimental data (Fig. 2). The stress relaxation constants ($\alpha = 7.2$, $\beta = 423.5$, $\lambda = 0.11$, $a = 1.35$) corresponds to the first relaxation step at a pre-stress of 600 MPa (refer Table A.1) and were obtained by least square fitting using Eq. (23) explained in the subsequent section. The evolution of forward and reverse dislocation density during stress relaxation (Eqs. (18) and (21)) for typical values of $\Gamma = 0.35$ and $q = 0.5$ is shown in Fig. 3.

Experimental observation suggests that most of the stress drop during relaxation occurs within the first few seconds. Therefore, the annihilation is expected to dominate the initial period. The value of θ_r depends upon the choice of Γ and q, as shown in Fig. 4. Γ was varied between $0 < \Gamma < 1$ as they represent the extreme cases. Larger value of q leads to negative value of θ_r (Fig. 5). While the theoretical possibility of negative θ_r cannot be ruled out (Mohebbi et al., 2015), typical cases suggest that it involves significant annihilation of ρ_m. Therefore, it is reasonable to assume that $\theta_r > 0$ for most cases.

θ_r predicted for the above experimental data is plotted (Fig. 4) as a function of Γ and q; θ_r increases with Γ or q or both. The rate of hardening ($\theta = d\sigma/d\varepsilon$) from the monotonic tensile test data at the relaxation pre-stress is compared along with θ_r in Fig. 5. One of the important inferences from the analysis is that $\theta_{r(max)} < \theta$ even when there is no dislocation annihilation (Γ or $q = 0$). This is a direct consequence

Table 1
Material constants obtained by least square fitting of SS 316.

M	φ	μ[GPa]	b[nm]	m	K_1	K_2	$\dot{\varepsilon}_0$[s^{-1}]	ρ_0[mm^{-2}]
3	0.563	85	0.247	0.096	46,000	3.28	7.85×10^{-6}	3.07×10^{7}

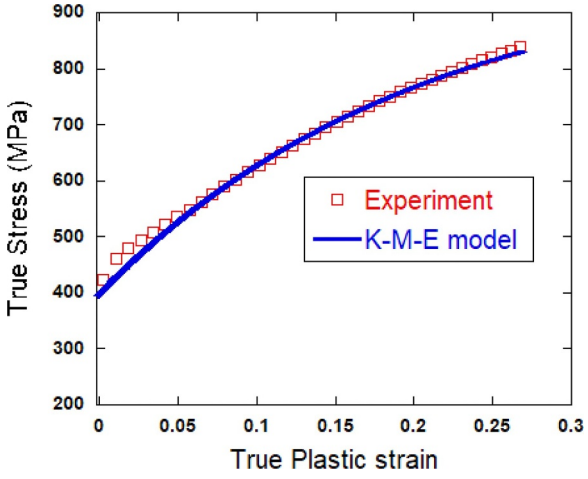

Fig. 2. Stress-strain curve obtained using KME model compared with experimental data of SS 316.

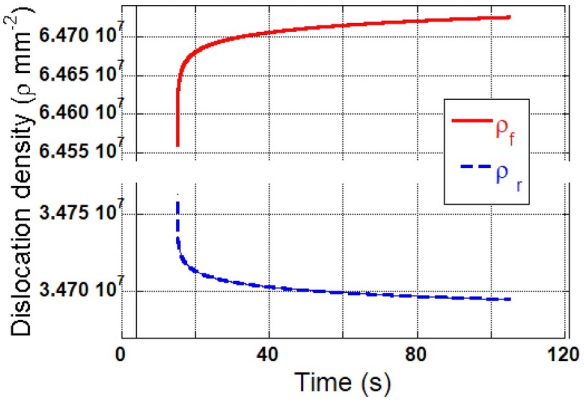

Fig. 3. Evolution of forward and reverse dislocations during stress relaxation, assuming $\Gamma = 0.35$ and $q = 0.5$ in SS 316.

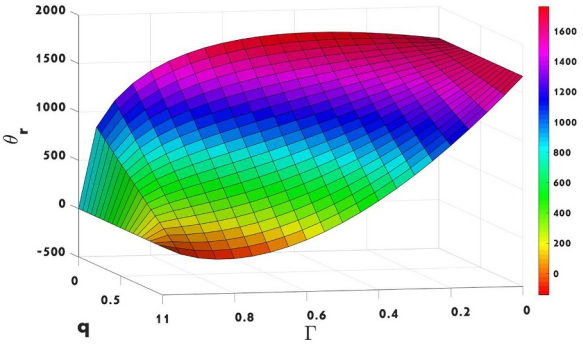

Fig. 4. Variation of θ_r with Γ and q for SS 316 investigated in the present work.

of K-M-E model, as shown below. From Eq. (15),

$$\Delta\sigma = \Delta\sigma_i(\dot{\varepsilon}/\dot{\varepsilon}_0)^m \tag{22}$$

Therefore for a given strain increment ($\Delta\varepsilon$), $\theta/\theta_{r(max)} = (\dot{\varepsilon}/\dot{\varepsilon}_0)^m$. The quantity $(\dot{\varepsilon}/\dot{\varepsilon}_0)^m > 1$ for any $\sigma > \sigma_i$.

The net value of σ_i at any instance is due to the combined effect of ρ_f and ρ_r. It's evolution for the above case is shown in Fig. 6. To understand the influence of ρ_r, a theoretical case assuming $\rho_r = 0(\Gamma = 0)$ is plotted along with. This corresponds to the maximum increase in σ_i during relaxation. The overall change in $\Delta\sigma_i$ is negligible. Therefore, the difference between subsequent relaxation steps is primarily due to change in ρ_m and not due to σ_i as attributed in Sargent et al. (1969).

Modeling strain hardening during stress relaxation is still an open

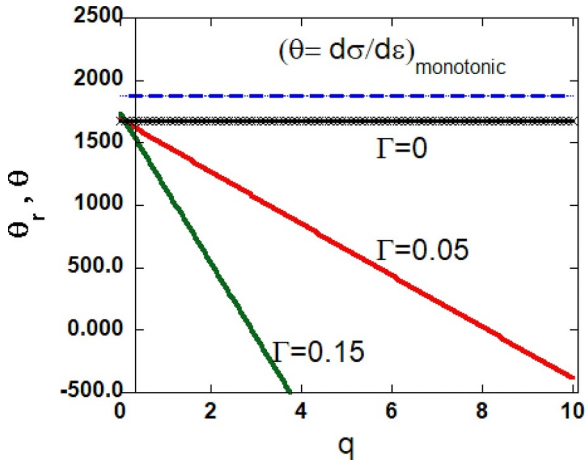

Fig. 5. θ_r decreases with q. Large values of q leads to $-$ve values in SS 316. $\theta_r < \theta$ in all the cases.

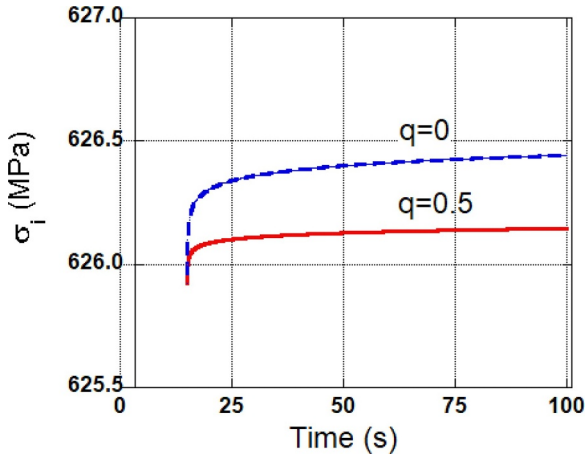

Fig. 6. Evolution of internal stress during stress relaxation ($\Gamma = 0.35$) of SS 316.

problem (Caillard and Martin, 2003). Since both strain hardening and reduction of mobile dislocation density result in similar macroscopic behavior, it is not possible to decouple them without additional tests. It is therefore recommended to estimate θ_r from curve fitting bounded in the range of $0 < \theta_r < \theta_{r(max)}$. Eq. (13) can be modified to account for the internal stress change as follows,

$$\sigma_0 - \sigma = \bar{\alpha}\, ln\left[1 + \bar{\beta}\left\{\left(\frac{t+a}{a}\right)^{1-\lambda} - 1\right\}\right] \tag{23}$$

where $\bar{\alpha} = \alpha\left(\frac{1+\theta_r}{E}\right)$.

Both θ_r and λ in the above equation has a similar effect on stress relaxation and cannot be separated. One of the possibilities (described in Caillard and Martin, 2003) is to assume $\theta_r = \theta$. Although, $(\theta_r)_{actual} \neq \theta$, the assumption is reasonable as $\Delta\sigma_i \ll \Delta\sigma$.

2.2. Estimation of activation volume

As discussed earlier, estimation of activation volume from single relaxation test will yield only an apparent value (V_a) due to the dynamic nature of ρ_m and σ_i. Spätig et al. (1993) (model 1) used repeated relaxation to estimate the actual activation volume for logarithmic model. Repeated relaxation is characterized by a pre-stress, σ_0 to which the specimen is immediately reloaded between successive relaxation steps. This reloading is assumed not to alter the substructure and therefore is expected not to change either ρ_m or σ_i.[3] Based on this assumption, V^* for model 1 is given (refer Section A.4.1) by Eq. (24) and shall be referred as method-1.

$$V^* = \left(\frac{-kT}{\Delta\sigma_j}\right) ln\left(\frac{\beta_{j+1}(1+\beta_j t)}{\beta_j}\right) \tag{24}$$

where subscript j refers to the relaxation step.

An alternate procedure for estimating activation volume can be found in Martin et al. (2002) where the strain rate ratio within a single relaxation step is estimated using the apparent activation volume, $V_a = \Omega V^*$. This method shall henceforth be referred as method-2. The ratio of strain rate at the beginning of two consecutive relaxations is given (Section A.4.2) by

$$\frac{\dot{\varepsilon}_{p(i,j+1)}}{\dot{\varepsilon}_{p(i,j)}} = exp\left[(\Omega - 1)V^*\Delta\sigma_j/kT\right] \tag{25}$$

where subscript i refers to the initial condition of relaxation step.

Eq. (25) can be extended to relate the first and nth relaxation step as

$$\frac{\dot{\varepsilon}_{p(i,n)}}{\dot{\varepsilon}_{p(i,1)}} = exp\left\{(\Omega - 1)V^* \sum_{1}^{n-1} (\Delta\sigma_j/kT)\right\} \tag{26}$$

The strain rate ratio for a single relaxation step through Eq. (25) is valid only if $ln(\dot{\varepsilon}_p)$ vs. $\Delta\sigma$ exhibits a linear relation during relaxation, which is complied by model 1. However, as mentioned earlier, accounting the mobile dislocation density change require either time dependent variation of β or an alternative mathematical form. It is less likely to obtain a linear relation when such modifications are attempted. Therefore, it is not recommended to use the method-2 to estimate V^*.

2.2.1. V^* For the proposed model

The new model in the present work exhibits non-linear relation between $ln(\dot{\varepsilon}_p)$ and $\Delta\sigma$, as expected. Therefore, method-1 is used to derive V^* using the proposed model. Substituting $\dot{\varepsilon}$ from Eq. (17) and simplifying,

$$\frac{\dot{\varepsilon}_{p(i,j+1)}}{\dot{\varepsilon}_{p(f,j)}} = \frac{\psi_{i,j+1}}{\psi_j}\frac{(t+a_j)_j^{\lambda}}{(a_{j+1})_{j+1}^{\lambda}}\left[1 + \bar{\beta}_j\left\{\left(\frac{t+a_j}{a_j}\right)^{1-\lambda_j} - 1\right\}\right]$$

V^* for the proposed model can be estimated following the procedure in Section A.4.1 as

$$V^* = \left(\frac{-kT}{\Delta\sigma_j}\right) ln\left(\frac{\psi_{j+1}}{\psi_j}\frac{(t+a_j)_j^{\lambda}}{(a_{j+1})_{j+1}^{\lambda}}\left[1 + \bar{\beta}_j\left\{\left(\frac{t+a_j}{a_j}\right)^{1-\lambda_j} - 1\right\}\right]\right) \tag{27}$$

3. Experiments

Repeated stress relaxation under monotonic tension in a commercially available marine grade low carbon stainless steel, SS 316L was studied using a 30 kN tensile testing machine (Zwick/Roell Z030 with an optical extensometer). The chemical composition and mechanical properties of the material are tabulated in Table 2 and Table 3 respectively. The specimens were prepared according to ASTM E8 standard. The experiments were carried out by interrupting the monotonic tensile test at predefined stress level between 550 MPa and 640 MPa. Around 10 relaxation steps of 30 s hold time were performed in each trial. The effect of hold time was studied by performing additional experiments with 10 s and 60 s. All the experiments were carried out at a strain rate of 10^{-2} s^{-1} and were repeated with at least three samples.

[3] In the original reference (Spätig et al., 1993; Caillard and Martin, 2003), there is no mention of the constancy in internal stress. However, $\Delta\sigma$ replaced $\Delta\sigma^*$, which is possible only when σ_i remains invariant.

Table 2
Chemical composition- SS 316.

Element	C	Mn	S	P	Si	Cr	Ni	Fe
SS316L	0.02	1.70	0.003	0.04	0.30	17.10	10.0	Rem

Table 3
Mechanical properties- SS 316.

Grade	ν	E[GPa]	YS, $R_{p0.2}$[MPa]	UTS[MPa]	Total elongation [%]
SS316L	0.25	193	415	639	42.2

relaxation[4] tests (Hariharan et al., 2013; Eipert et al., 2014; Li et al., 2017). However, contrary to the results of single step relaxation (Hariharan et al., 2016; Prasad et al., 2018), no ductility improvement is observed as the hold time increased from 10 to 60 s (Fig. 7d).

Fig. 8 shows the variation of stress with time during repeated relaxation. The total stress drop during relaxation decreases with progression of relaxation steps. The magnitude and trend of stress drop is dependent on relaxation time and pre-stress (Fig. 8b and c). The trend observed in Fig. 8b is similar to that reported earlier (Hariharan et al., 2013). The stress drop during relaxation, in general increased with the pre-stress, except at 640 MPa. The reversed trend at 640 MPa could possibly be due to the corresponding plastic strain that had crossed the

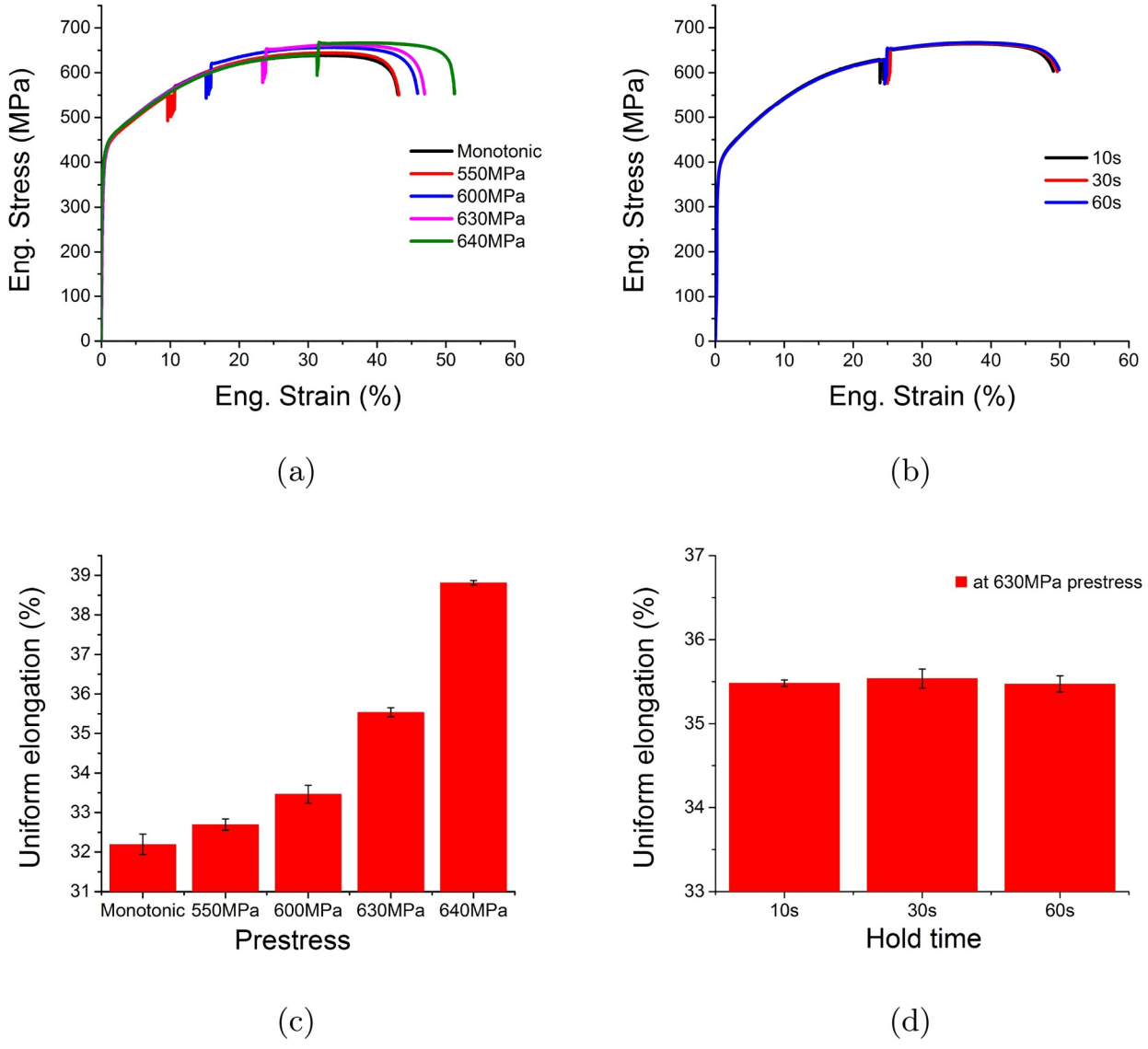

Fig. 7. (a) Ductility improvement in SS 316 during repeated stress relaxation at different pre-stress; (b) Engineering Stress strain curve- repeated relaxation at 630MPa for varying hold time; Effect of initial stress (c) and relaxation time (d) in the improvement of uniform elongation during repeated stress relaxation.

4. Results and discussion

Typical stress-strain curve obtained during repeated relaxation tests is shown in Fig. 7a and b. Repeated relaxation increases the overall ductility of the material. The ductility improvement increases with pre-strain (stress)(Fig. 7c), similar to the trend observed in single (Hariharan et al., 2016; Prasad et al., 2018) and multiple plastic instability (ultimate tensile strength). The ductility improvement during stress relaxation is attributed (Hariharan et al., 2016; Varma et al., 2018) to the net effect of two simultaneously active mechanisms,

[4] The flow stress at the beginning of every individual relaxation step is constant during repeated relaxation. Such restriction is not imposed in multiple relaxation and the material strain hardens between subsequent relaxation steps.

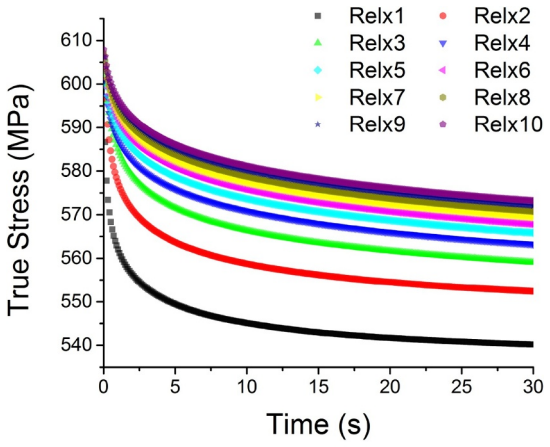

(a)

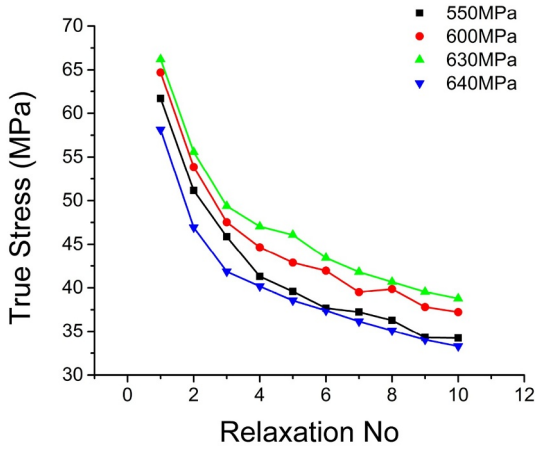

(b)

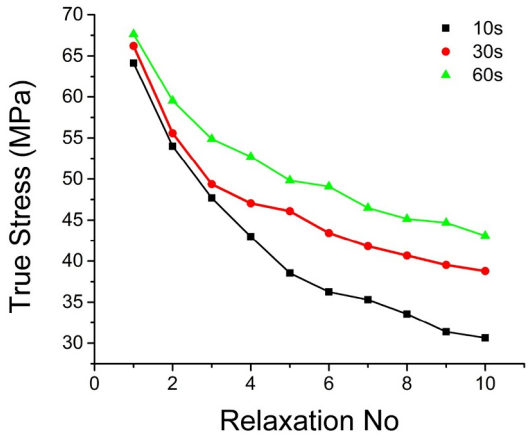

(c)

Fig. 8. Stress drop decrease continuously with number of relaxation steps during repeated relaxation in SS 316: (a) Stress vs. time trend during repeated stress relaxation at 550 MPa, (b) Effect of pre-stress and (c) Effect of relaxation time (pre-stress- 630 MPa).

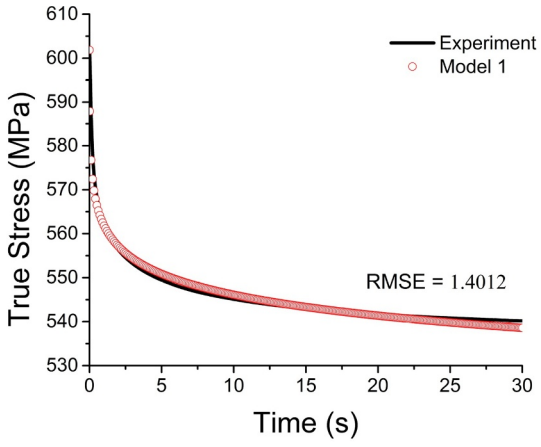

(a)

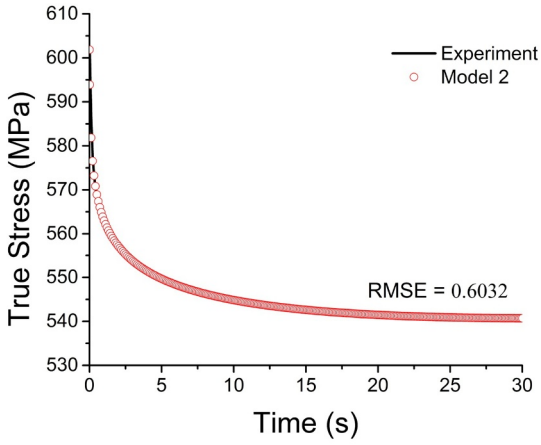

(b)

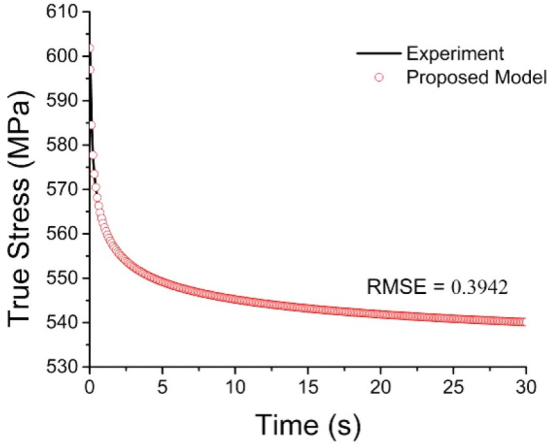

(c)

Fig. 9. Comparison of different models to fit the experimental data of SS 316 during stress relaxation at 550 MPa and 30 s. Data fit of single relaxation step using (a) model 1 (b) model 2 and (c) proposed model.

namely (i) dislocation annihilation and (ii) homogenization of internal stress. The initial few seconds is dominated by annihilation mechanism whereas the improvement at longer time intervals is contributed by the internal stress homogenization.

During repeated relaxation test, the end of first relaxation step witnesses reduced mobile dislocation density and homogeneous internal stress. When the material is reloaded to σ_0, the dislocation

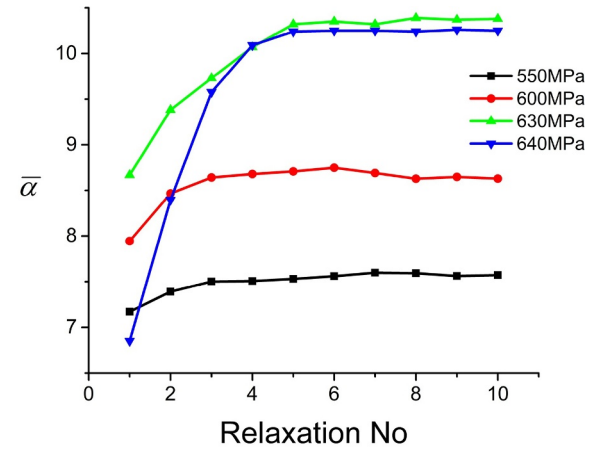

(a)

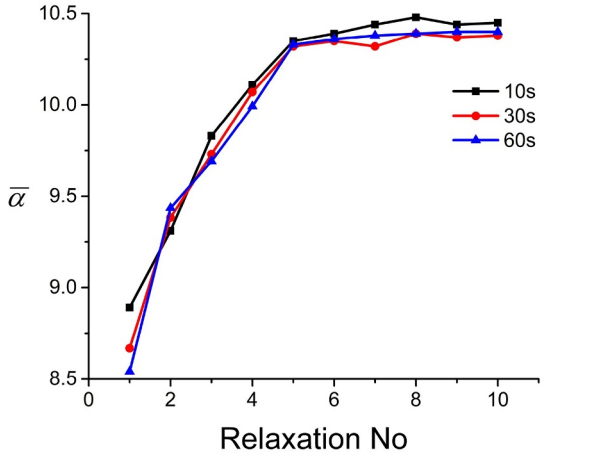

(b)

Fig. 10. Variation of $\bar{\alpha}$ with (a) pre-stress and (b) time in SS 316. $\bar{\alpha}$ increases initially and saturate after 5 relaxation steps.

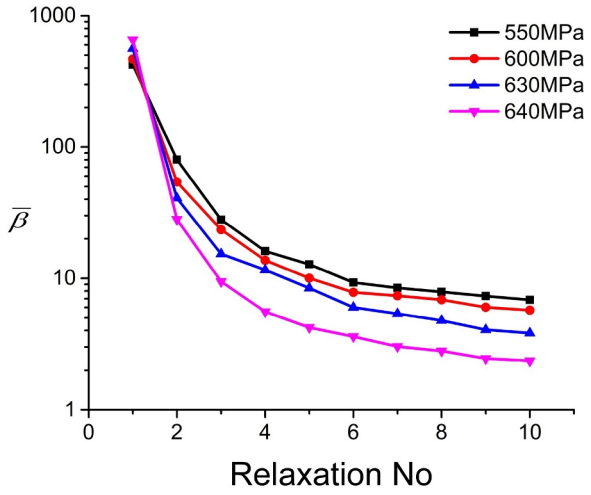

(a)

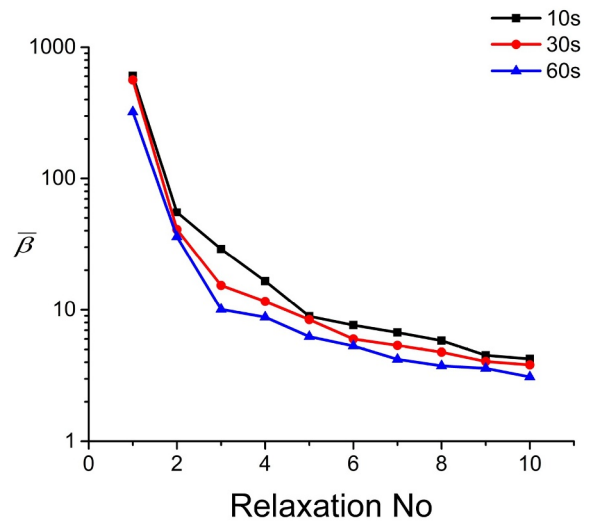

(b)

Fig. 11. Effect of (a) pre-stress and (b) time on the variation of $\bar{\beta}$ with relaxation steps in SS 316.

density does not increase. Assuming the increase in ρ_m due to strain hardening is negligible, the mobile dislocation density available for annihilation at the beginning of second relaxation step must be less than that during the initiation of first relaxation step. With the increment in repeated relaxation steps, the annihilation of ρ_m will subside completely.

4.1. Validation of the proposed model

The first relaxation step of repeated relaxations performed at 550 MPa and 30 s hold time was fit using models 1, 2 and the proposed model. The constants of the model were identified by least square fit of the experimental data using commercial software, MATLAB. The fit data are tabulated in Section A.5. Model 2 and the proposed model are extensions of the logarithmic model (model 1). The values of α and β obtained while fitting model 1 were used as initial guess in estimating the parameters for model 2 and the proposed model. All three models fit the experimental data with reasonable accuracy (Fig. 9). It is observed that the root mean square error (RMSE) in prediction is least for the proposed model followed by model 2 and 1. The improved accuracy can be attributed to the flexibility introduced by additional constants in the proposed model.

The proposed model was used to fit all the repeated relaxation data obtained from the experiments. Each relaxation step in repeated relaxation was fit independently. α in model 1 represents the combined transient effect of σ_i and ρ_m and was treated (Caillard and Martin, 2003) constant during repeated relaxation. Unlike model 1, $\bar{\alpha}$ in the proposed model accounts only for $(\sigma_i)_t$ (refer Section 2.1). No constraint was imposed on the constancy of $\bar{\alpha}$ while fitting the experimental data.

It is observed from Fig. 10 that $\bar{\alpha}$ increase upto five relaxation steps and saturates to a constant value.∵ $\bar{\alpha} = \alpha\left(\frac{1+\theta_r}{E}\right)$, it may be concluded that θ_r too reaches a stable value after fifth relaxation step. $(\sigma_i)_t$ is non-linear due to the combined effect of dislocation annihilation and work hardening; of which σ_i decreases due to the former and increases with the latter. The constancy in θ_r after fifth relaxation step suggests that $(\sigma_i)_t$ is only due to work hardening and dislocation annihilation after fifth relaxation step is negligible. The reduction of ρ_m after the fifth relaxation step could be due to its conversion to sessile dislocation at the obstacles. $\bar{\alpha}$ is inversely proportional to the apparent activation volume and hence its trend with stress and time shall be discussed along with activation volume in the subsequent paragraphs.

The constant $\bar{\beta}$ is related to (a) mobile dislocation density at the beginning of relaxation step (ρ_{m0}) and (b) λ. ρ_{m0} increases with pre-

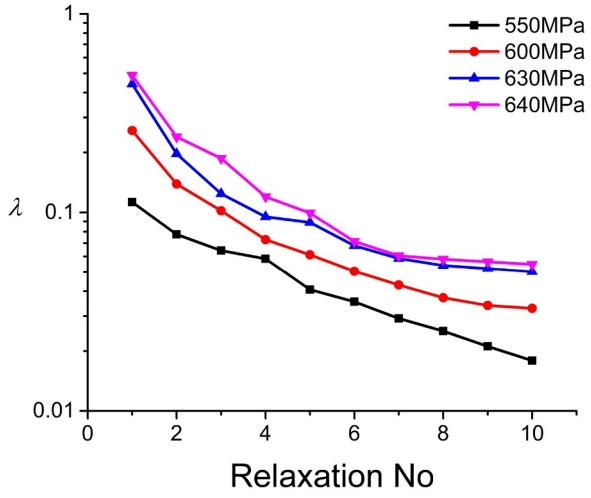

(a)

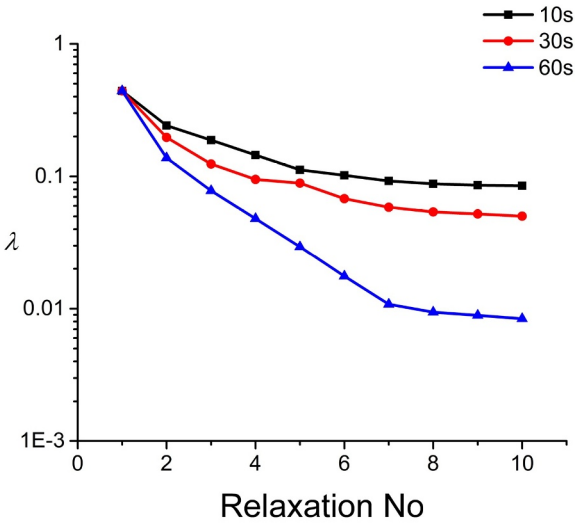

(b)

Fig. 12. Variation of λ with (a) pre-stress and (b) relaxation hold time in SS 316.

strain (stress) in monotonic loading due to strain hardening. The correlation with $\bar{\beta}$ is evident that its value increased with pre-stress in the first relaxation step (Fig. 11a). However, the trend got reversed in subsequent relaxation steps due to its dependence on λ. The relaxation time had little effect on $\bar{\beta}$ (Fig. 11b) suggesting that the decrease of mobile dislocation density is complete within shorter time intervals (less than 10s). This is consistent with the findings on the mechanism related to stress relaxation (Hariharan et al., 2016; Varma et al., 2018). The constant, λ which refers to the rate of reduction of mobile dislocation density was observed to increase with pre-stress (Fig. 12a). Since ρ_{m0} increases with pre-stress, it may be concluded that λ is dependent upon ρ_{m0}. A similar trend of increase in the rate of reduction of ρ_m with stress was reported by Okazaki et al. (1976). As the relaxation time increases, the internal stress homogenize (Hariharan et al., 2016; Varma et al., 2018; Wang et al., 2017) reducing the stress concentration zones in the lattice. The inhomogeneous internal stress and the stress concentration zones serve as driving force for dislocation annihilation. They also assist in reduction of ρ_m by entrapment at the obstacle interface. The rate of reduction of ρ_m decreases at longer time intervals with internal stress homogenization, evident from Fig. 12b.

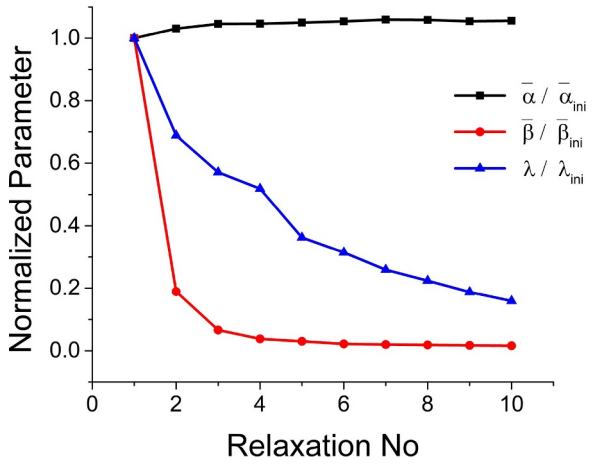

Fig. 13. Relative variation of $\bar{\alpha}$, $\bar{\beta}$ & λ normalized with their initial values. The subscript 'ini' in the legend indicates the initial value at first relaxation step. Material - SS 316.

The relative variation of the three parameters ($\bar{\alpha}$, $\bar{\beta}$ & λ) with respect to their initial values (1st relaxation step) is plotted in Fig. 13. It is observed that $\bar{\alpha}$ is relatively invariant, in agreement with the constraint imposed in model 1. It was inferred in the discussion of $\bar{\alpha}$ that the dislocation annihilation subside after fifth relaxation step and the reduction of ρ_m in subsequent steps could be due to conversion of mobile to sessile dislocations. Similar conclusion could be arrived from the trend of $\frac{\bar{\beta}}{(\bar{\beta})_{ini}}$ and $\frac{\lambda}{(\lambda)_{ini}}$, as both vary non-linearly till the fifth relaxation step (Fig. 13). The non-linearity is due to the combined effect of dislocation annihilation and strain hardening on ρ_m whereas the linear portion post fifth relaxation step indicates the contribution to be purely by strain hardening. $\frac{\lambda}{(\lambda)_{ini}}$ drastically reduces to near saturation in the first two relaxation steps. Since λ indicates the rate of annihilation, it is clear that maximum dislocation annihilation occurs in the first relaxation step. It is worth mentioning that the ductility improvement due to stress relaxation is maximum in the first relaxation step. The improvement is only marginal in subsequent relaxation steps. It provides an indirect evidence that dislocation annihilation plays a vital role in ductility improvement due to stress relaxation.

The activation volume V^* is calculated using Eq. (27) and its dependence on stress and relaxation time are shown in Figure. 14a & 14b. The estimated activation volume in first relaxation step was in the range of 8.5–14 b^3. The activation volume initially increased and saturated with relaxation steps. The activation volume in tenth relaxation step was in the range of 26–33 b^3. The saturated values of V^* is plotted as a function of stress and time respectively in Fig. 14c and d. The estimated V^* is consistent with the range reported in literature (Campbell et al., 1977).

A similar observation of activation volume increasing with relaxation steps was made by Yang et al. (2006) for repeated stress relaxation in nanostructured copper. Lower activation volumes are observed at higher predefined stress levels and is consistent with earlier observations (Spätig et al., 1993; Martin et al., 2002). At a given relaxation step, V^* decreases with increase in pre-stress. This trend correlates inversely with $\bar{\alpha}$ (Fig. 10a) and directly with $\bar{\beta}$ (Fig. 11a). $\bar{\alpha}$ and $\bar{\beta}$ respectively accounts for the transient effect of σ_i and ρ_m. From Fig. 13, the variation of $\frac{\bar{\alpha}}{(\bar{\alpha})_{ini}}$ with relaxation step is much less than that of $\frac{\bar{\beta}}{(\bar{\beta})_{ini}}$, suggesting $\Delta\sigma_i$ has relatively lesser influence on the estimation of V^* when compared to ρ_m. The evolution of V^* is also influenced by the relaxation hold time (Fig. 14b). With increase in relaxation hold time, V^* saturates with lesser number of relaxation steps.

The activation volume usually decreases with strain hardening, evident from Fig. 14a. The increase in activation volume during repeated relaxation suggests work softening. At any given relaxation step

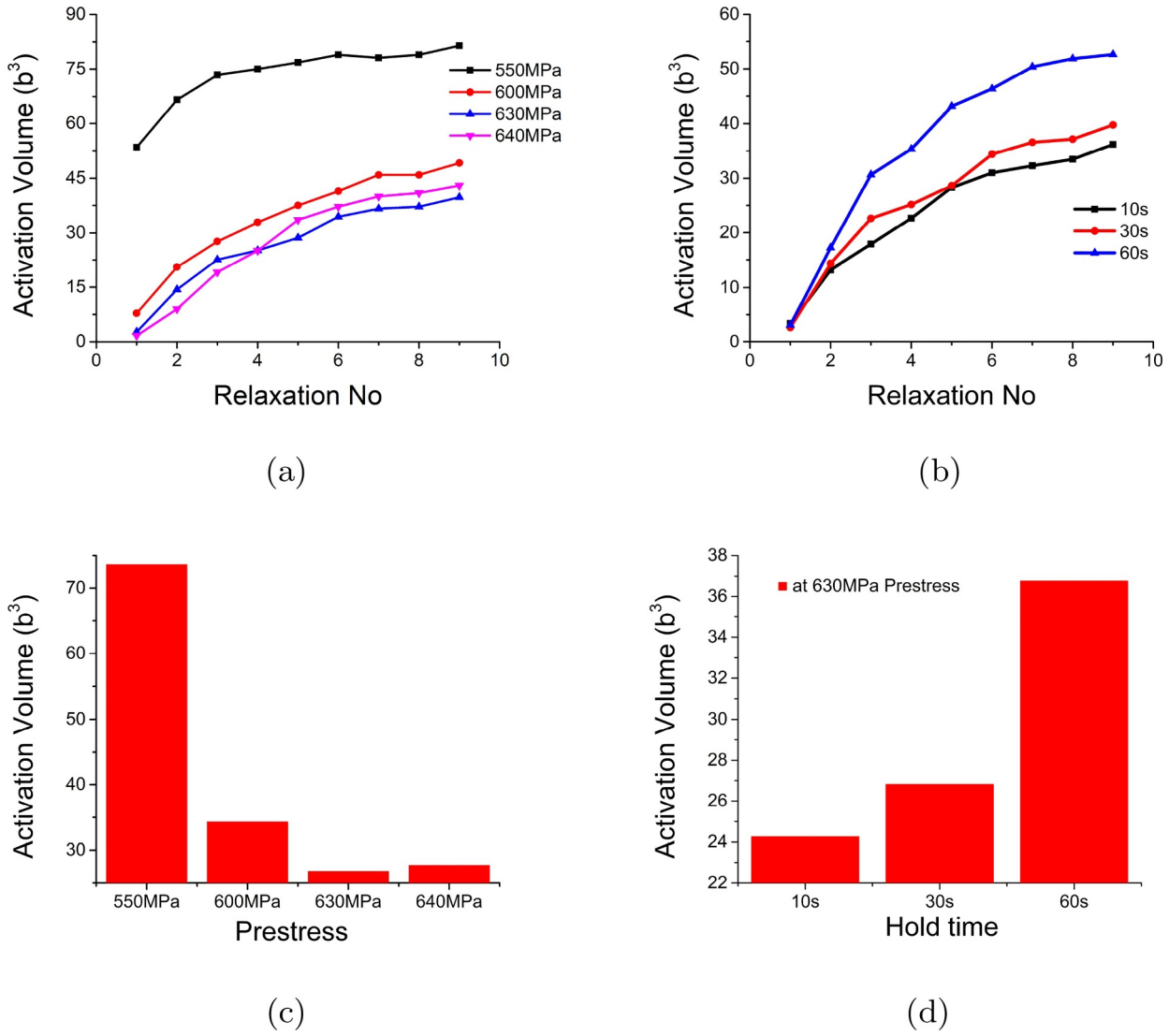

Fig. 14. Effect of (a) stress and (b) relaxation hold time on the evolution of activation volume in SS 316. V^* saturates with the relaxation steps. The effect of (c) stress and (d) relaxation hold time on the saturated value of V^*.

prior to saturation, V^* increases with hold time (Fig. 14b). Thus work softening occurs with increase in relaxation steps and hold time. This may appear counter-intuitive as we have shown that the material strain hardens (although infinitesimally) during relaxation. However, overall softening is still possible if the internal stress tend to homogenize within the lattice, thereby relieving the stress concentration zones. The above observations and the plausible explanation are in agreement with the mechanism of internal stress homogenization proposed recently (Hariharan et al., 2016; Varma et al., 2018) to explain the observed ductility improvement due to stress relaxation.

5. Conclusion

Repeated stress relaxation test is a useful macroscopic test to estimate the activation parameters. The variation of mobile dislocation density is not modeled accurately in the logarithmic model. It is shown that extending the logarithmic model without any modification of the constant 'β' conflicts with the inherent assumption of constant ρ_m. Although this does not cause serious error in fitting the experimental data, the activation volume calculated using the model is inaccurate. An advanced phenomenological model is proposed in the present work, which overcomes the limitation of the existing model. In addition to modeling evolution of mobile dislocations, the proposed model adopted dislocation density based approach to account for the evolution of transient internal stress. This attempt is probably unique in the modeling of stress relaxation. The experimental results obtained from SS316 material are used to compare the proposed model with other existing models. The accuracy of data fitting using the proposed model is found to be improved when compared with the existing models. In a typical single stress relaxation test, the RMSE of the proposed model is 0.4 against 1.4 for the traditional logarithmic model. While the dependence on least square fitting method to identify all the constants in the proposed model is a limitation, it can be overcome when additional experiments are developed in future to understand the physical nature of constants.

Acknowledgments

One of the authors (K.H.) would like to acknowledge the support received from Department of Science & Technology (DST) India through the SERB project no. YSS/2015/001342. MGL appreciates partial support from National Foundation of Korea (NRF-2017R1A2A2A05069619/2012R1A5A1048294). FB is grateful to POSCO for generous support.

Appendix A

A1. Integration of proposed logarithmic model

Eq. (12) can be simplified as

$$-\frac{d\sigma}{dt} = C_1 a^{\lambda}(t+a)^{-\lambda}\, exp(C_2\sigma) \tag{A.1}$$

where $C_1 = E\phi b\rho_{m0}\exp\left(-\frac{\Delta G_0 + \sigma_i V^*}{kT}\right)$ and $C_2 = \frac{V^*}{kT}$.

Rearranging and integrating Eq. (A.1)

$$exp(-C_2\sigma) = \frac{C_2 C_1 a^{\lambda}(t+a)^{1-\lambda}}{1-\lambda} + C_2 D \tag{A.2}$$

where D is the integration constant, which can be obtained by substituting $\sigma = \sigma_0$ at $t = 0$ in Eq. (A.2).

$$C_2 D \;= exp(-C_2\sigma_0) - \frac{C_2 C_1 a}{1-\lambda}$$

Substituting C_2D back in Eq. (A.2) and simplifying,

$$exp(-C_2\sigma) \;= exp(-C_2\sigma_0)\left[1 + \frac{C_2 C_1 a}{1-\lambda} exp(C_2\sigma_0)\left\{\left(\frac{t+a}{a}\right)^{1-\lambda} - 1\right\}\right] \tag{A.3a}$$

$$\sigma_0 - \sigma \;= \frac{1}{C_2}\left[1 + \frac{C_2 C_1 a}{1-\lambda} exp(-C_2\sigma_0)\left\{\left(\frac{t+a}{a}\right)^{1-\lambda} - 1\right\}\right] \tag{A.3b}$$

Substituting C_1 and C_2 in Eq. (A.3b),

$$\sigma_0 - \sigma = \alpha\, ln\left[1 + \bar{\beta}\left\{\left(\frac{t+a}{a}\right)^{1-\lambda} - 1\right\}\right] \tag{A.4}$$

where

$$\alpha \;=\; kT/V^*$$

$$\bar{\beta} \;=\; E\phi b\rho_{m0}\frac{V^*}{kT}\frac{a}{1-\lambda}\exp\left(-\frac{\Delta G_0 - \sigma_0{}^* V^*}{kT}\right)$$

$\sigma_0{}^*$ refers to the effective stress at the beginning of relaxation ($t = 0$).

A2. Forward and reverse dislocations

Let the total dislocation density at pre-strain, ε_0 be indicated as $(\rho)_{\varepsilon_0} = \tilde{\rho}$. $\tilde{\rho}$ is contributed by both mobile (ρ_m) and immobile dislocations (ρ_{im}).

$$\tilde{\rho} = \rho_{m(t=0)} + \rho_{im(t=0)} \tag{A.5}$$

The evolution of total dislocation density with time (ρ_t) is due to the superposition of mechanisms that control the evolution of mobile and immobile dislocations in the lattice (Eq. (A.6a)). As discussed earlier, the mobile dislocation density reduces during stress relaxation. The reduction of ρ_m is due to the combined effect (Eq. (A.6b)) of dislocation annihilation and the immobilization at the obstacle interface.

$$\rho_t \;= \rho_{m(t=0)} + \rho_{im(t=0)} - \Delta\rho_{m(t)} + \Delta\rho_{im(t)} \tag{A.6a}$$

$$-\Delta\rho_{m(t)} \;= \Delta\rho_{m(trap)} - \Delta\rho_{m(anni)} \tag{A.6b}$$

where $\Delta\rho_{m(trap)}$ indicates the immobilization of fraction of mobile dislocations by the obstacles and $\Delta\rho_{m(anni)}$ indicates the annihilation. Since the latter reduces the total dislocation density, negative sign is used for the component.

In addition to the above, strain hardening driven by the plastic strain increment during stress relaxation, $(\Delta\varepsilon_p)_t$ increases the total dislocation density.

$$\Delta\rho_{SH(t)} = \Delta\rho_{m(SH)} + \Delta\rho_{im(SH)} \tag{A.7}$$

where the subscript SH indicates strain hardening. Summarizing the different contributions to transient total dislocation density during stress relaxation,

$$\Delta\rho_t = \Delta\rho_{m(SH)} + \Delta\rho_{im(SH)} + \Delta\rho_{m(trap)} - \Delta\rho_{m(anni)} \tag{A.8}$$

All the components of dislocation density increment with the exception of annihilation $\Delta\rho_{m(anni)}$ contributes positively to the increase in total dislocation density during subsequent deformation. Therefore the time dependent evolution of ρ can be grouped into forward (ρ_f) and reverse dislocation (ρ_r) densities,

$$\rho_t = \rho_f + \rho_r \tag{A.9}$$

where ρ_f and ρ_r respectively indicates forward and reverse dislocation densities given by $\rho_f = \Delta\rho_{m(SH)} + \Delta\rho_{im(SH)} + \Delta\rho_{m(trap)}$ and $\rho_r = -\Delta\rho_{m(anni)}$.

A3. Orowan mechanism for stress relaxation

The plastic deformation is accomplished by the movement of dislocations from one equilibrium state to other, crossing a thermal energy barrier. The dislocations move discreetly spending a characteristic wait time at the obstacles (Barlat et al., 2002). At any instant during plastic deformation, statistically, there are many dislocation line segments that are perturbed from their equilibrium position but possess insufficient energy to cross the thermal barrier. During stress relaxation, the plastic strain rate decreases continuously and it decreases the probability of dislocation segments crossing the thermal barrier. Therefore, such dislocations try to reach their initial equilibrium state from which they were perturbed. Physically, the scenario can be imagined by considering an initially straight edge dislocation line(shown as A in Fig. A.1a passing through a set of obstacles in the

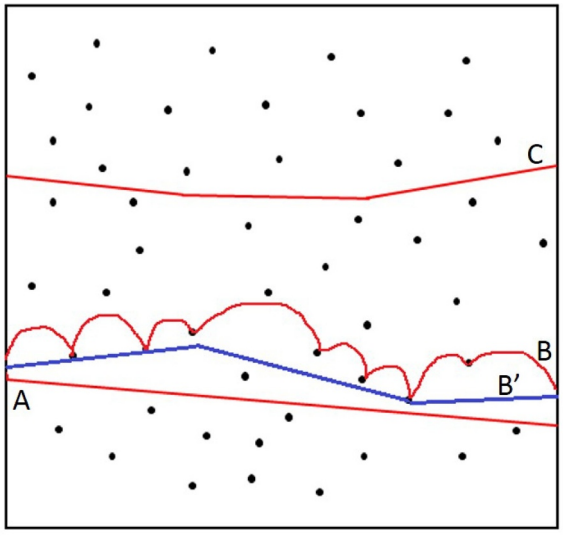

(a) Dislocation segment A and C are in equilibrium whereas dislocation segment B is trapped between obstacles. During relaxation, dislocation segment B tends to come back to equilibrium, B'

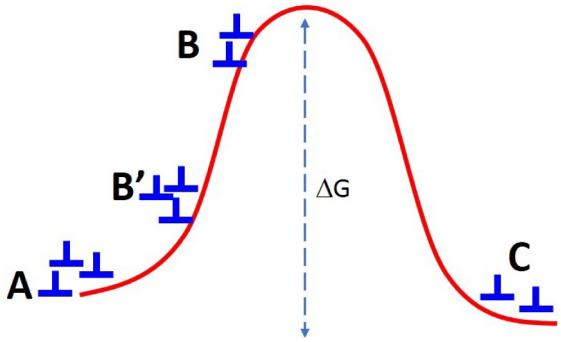

(b) Dislocation segments A and C are separated by energy barrier ΔG. During relaxation, the dislocation segment B moves to B' in its attempt to reach equilibrium

Fig. A1. Schematic illustration of dislocation annihilation during stress relaxation.

crystal lattice. The dislocation movement follows Orowan mechanism of pinning around the obstacles before traversing them. The dislocation segment A and C (Fig. A.1b) are in equilibrium state, C has crossed a set of obstacles whereas A has not been moved from its initial equilibrium. During stress relaxation, the dislocation segment B, which has not crossed the obstacles will be unpinned and try to straighten out like A. In this process the dislocation segments loses their kinetic energy due to reduction of average dislocation velocity, which provides sufficient driving force for dislocation annihilation when interacting with the other moving dislocations of opposite sign.

A4. Methods to estimate activation volume

It is assumed that ρ_m remain invariant between the end of a stress relaxation step and the onset of subsequent relaxation (Caillard and Martin, 2003). Derivation of V^* using this assumption is referred as method-1.

A4.1. Method 1

From Orowan equation, $\dot{\varepsilon}$ at the end of a relaxation step and the beginning of next relaxation step is governed only by the average dislocation velocity.

$$\frac{\dot{\varepsilon}_{p(i,j+1)}}{\dot{\varepsilon}_{p(f,j)}} = \frac{v_{(i,j+1)}}{v_{(f,j)}} = exp(-V^*(\sigma^*_{(i,j+1)} - \sigma^*_{(f,j)})/kT) \tag{A.10}$$

where the subscript '*i*' and '*f*' indicates the initiation ($t = 0$) and end of relaxation. The subscript '*j*' refers to the stress relaxation step. Rewriting the above equation,

$$\frac{\dot{\varepsilon}_{p(i,j+1)}}{\dot{\varepsilon}_{p(f,j)}} = exp(-V^*\Delta\sigma_j/kT) \tag{A.11}$$

The strain rate ratio in the L.H.S of Eq. (A.11) when computed using model 1, reduces to

$$\frac{\dot{\varepsilon}_{p(i,j+1)}}{\dot{\varepsilon}_{p(f,j)}} = \frac{-\alpha_{j+1}\beta_{j+1}}{1+\beta_{j+1}t} \Big/ \frac{-\alpha_j\beta_j}{1+\beta_j t} \tag{A.12a}$$

$$= \frac{\beta_{j+1}(1+\beta_j t)}{\beta_j} (\alpha_j = \alpha_{j+1} = \text{assumed constant}) \tag{A.12b}$$

From Eq. (A.11), V^* for model 1 is given by[5]

$$V^* = \left(\frac{-kT}{\Delta\sigma_j}\right) ln\left(\frac{\beta_{j+1}(1+\beta_j t)}{\beta_j}\right) \tag{A.13}$$

Following the above procedure, V^* for the proposed model can be derived as follows:
Substituting $\dot{\varepsilon}$ from Eq. (17) in the L.H.S of Eq. (A.11)

$$\frac{\dot{\varepsilon}_{p(i,j+1)}}{\dot{\varepsilon}_{p(f,j)}} = \frac{\psi_{j+1}}{\psi_j} \frac{(t+a_{j+1})^{\lambda}_{j+1}}{(t+a_j)^{\lambda}_j} \frac{1+\beta_j\left\{\left(\frac{t+a_j}{a_j}\right)^{1-\lambda_j} - 1\right\}}{1+\beta_{j+1}\left\{\left(\frac{t+a_{j+1}}{a_{j+1}}\right)^{1-\lambda_{j+1}} - 1\right\}} \tag{A.14a}$$

$$= \frac{\psi_{i,j+1}}{\psi_j} \frac{(a_{j+1})^{\lambda}_{j+1}}{(t+a_j)^{\lambda}_j} \left[1+\beta_j\left\{\left(\frac{t+a_j}{a_j}\right)^{1-\lambda_j} - 1\right\}\right] \tag{A.14b}$$

Simplifying and substituting in Eq. (A.11)

$$V^* = \left(\frac{-kT}{\Delta\sigma_j}\right) ln\left(\frac{\psi_{j+1}}{\psi_j} \frac{(a_{j+1})^{\lambda_{j+1}}}{(t+a_j)^{\lambda_j}} \left[1+\beta_j\left\{\left(\frac{t+a_j}{a_j}\right)^{1-\lambda_j} - 1\right\}\right]\right) \tag{A.15}$$

A4.2. Method 2

Unlike method 1, if the constancy of ρ_m is not imposed, V^* can be derived from a single relaxation step. This alternate procedure (Martin et al., 2002) is referred as method-2 in the present work. For this method, the variation in ρ_m and σ_i within a single relaxation step need to be considered. The strain rate ratio of *j*th relaxation step is given by

$$\frac{\dot{\varepsilon}_{p(i,j)}}{\dot{\varepsilon}_{p(f,j)}} = \frac{v_0 exp\left\{-\left(\frac{\Delta G_0 - V^*\sigma^*_{(i,j)}}{kT}\right)\right\}}{v_0 exp\left\{-\left(\frac{\Delta G_0 - V^*\sigma^*_{(f,j)}}{kT}\right)\right\}} = exp(-\Omega V^*\Delta\sigma_j/kT) \tag{A.16}$$

Since ρ_m and σ_i vary within a relaxation step, unlike method-1, apparent activation volume $V_a = \Omega V^*$ is used instead of V^*. Dividing Eq. (A.11) by Eq. (A.16) yields the ratio of strain rate at the beginning of two consecutive relaxations as

$$\frac{\dot{\varepsilon}_{p(i,j+1)}}{\dot{\varepsilon}_{p(i,j)}} = \frac{exp(-V^*\Delta\sigma_j/kT)}{exp(-\Omega V^*\Delta\sigma_j/kT)} = exp[(\Omega - 1)V^*\Delta\sigma_j/kT] \tag{A.17}$$

A5. Data obtained by curve fitting repeated relaxation results- SS 316

[5] The −ve sign in Eq. (24) is missing in the original references (Caillard and Martin, 2003; Martin et al., 2002).

Table A1
Stress variation: Model parameters for RSR carried out at 550 MPa (Engg. Stress) for hold time of 30 s.

Relaxation no.	$\bar{\alpha}$	$\bar{\beta}$	a	λ
1	7.171	423.5	1.347	0.1126
2	7.391	80.07	0.273	0.0752
3	7.501	27.97	0.0968	0.06428
4	7.506	16.11	0.0569	0.05839
5	7.53	12.77	0.04612	0.04078
6	7.56	9.281	0.03435	0.0354
7	7.598	8.449	0.03116	0.02917
8	7.593	7.879	0.02916	0.0252
9	7.562	7.314	0.0271	0.0211
10	7.572	6.846	0.0254	0.0179

Table A2
Stress variation: Model parameters for RSR carried out at 600 MPa (Engg. Stress) for hold time of 30 s.

Relaxation no.	$\bar{\alpha}$	$\bar{\beta}$	a	λ
1	7.944	467.2	1.3769	0.258
2	8.466	54.24	0.2024	0.139
3	8.64	23.48	0.088	0.102
4	8.679	13.71	0.0545	0.073
5	8.707	10.04	0.0414	0.0612
6	8.748	7.827	0.03267	0.0505
7	8.69	7.358	0.0306	0.043
8	8.627	6.87	0.0285	0.0371
9	8.647	6.019	0.02514	0.0339
10	8.628	5.72	0.02386	0.0328

Table A3
Stress variation: Model parameters for RSR carried out at 630 MPa (Engg. Stress)for hold time of 30 s.

Relaxation no.	$\bar{\alpha}$	$\bar{\beta}$	a	λ
1	8.668	562.5	1.363	0.442
2	9.382	40.83	0.1587	0.197
3	9.73	15.34	0.06538	0.124
4	10.07	11.58	0.0528	0.095
5	10.32	8.41	0.03896	0.089
6	10.35	6.004	0.02924	0.068
7	10.32	5.367	0.02607	0.0586
8	10.39	4.774	0.02324	0.054
9	10.37	4.052	0.0201	0.0521
10	10.38	3.828	0.01886	0.0502

Table A4
Hold time variation: Model parameters for RSR carried out at 630 MPa (Engg. Stress) for hold time of 10 s.

Relaxation no.	$\bar{\alpha}$	$\bar{\beta}$	a	λ
1	8.891	608	1.5082	0.442
2	9.31	55.25	0.2326	0.242
3	9.83	29	0.1264	0.188
4	10.11	16.54	0.0751	0.145
5	10.35	8.924	0.04192	0.112
6	10.39	7.65	0.0356	0.102
7	10.44	6.719	0.03183	0.0924
8	10.48	5.835	0.0279	0.088
9	10.44	4.52	0.0216	0.0859
10	10.45	4.245	0.0203	0.0851

Table A5
Hold time variation: Model parameters for RSR carried out at 630 MPa (Engg. Stress) for hold time of 30 s.

Relaxation no.	$\bar{\alpha}$	$\bar{\beta}$	a	λ
1	8.668	562.5	1.363	0.442
2	9.382	40.83	0.1587	0.197
3	9.73	15.34	0.06538	0.124
4	10.07	11.58	0.0528	0.095
5	10.32	8.41	0.03896	0.089
6	10.35	6.004	0.02924	0.068
7	10.32	5.367	0.02607	0.0586
8	10.39	4.774	0.02324	0.054
9	10.37	4.052	0.0201	0.0521
10	10.38	3.828	0.01886	0.0502

Table A6
Hold time variation: Model parameters for RSR carried out at 630 MPa (Engg. Stress) for hold time of 60s.

Relaxation no.	$\bar{\alpha}$	$\bar{\beta}$	a	λ
1	8.541	322.3	0.7688	0.442
2	9.435	35.97	0.1493	0.138
3	9.692	10.06	0.0475	0.078
4	9.992	8.795	0.0418	0.048
5	10.33	6.258	0.03137	0.0294
6	10.36	5.32	0.02702	0.0176
7	10.38	4.213	0.0217	0.0108
8	10.39	3.76	0.01932	0.0094
9	10.4	3.598	0.01854	0.0089
10	10.4	3.102	0.01599	0.0084

Table A7
Stress variation: Model parameters for RSR carried out at 640 MPa (Engg. Stress) for hold time of 30 s.

Relaxation no.	$\bar{\alpha}$	$\bar{\beta}$	a	λ
1	6.853	658.3	1.15264	0.489
2	8.396	28.08	0.0896	0.24
3	9.577	9.438	0.03673	0.187
4	10.09	5.564	0.0247	0.12
5	10.24	4.216	0.0195	0.0992
6	10.25	3.598	0.01711	0.0714
7	10.25	3.022	0.0147	0.0605
8	10.24	2.795	0.01348	0.0581
9	10.26	2.451	0.01186	0.0564
10	10.25	2.356	0.01141	0.0548

References

Anderson, P.M., Hirth, J.P., Lothe, J., 2017. Theory of Dislocations, Third ed. Cambridge University Press.

Babu, B., Lindgren, L.-E., 2013. Dislocation density based model for plastic deformation and globularization of Ti-6Al-4V. Int. J. Plast. 50, 94–108. https://doi.org/10.1016/j.ijplas.2013.04.003.

Barlat, F., Glazov, M.V., Brem, J.C., Lege, D., 2002. A simple model for dislocation behavior, strain and strain rate hardening evolution in deforming aluminum alloys. Int. J. Plast. 18 (7), 919–939. https://doi.org/10.1016/S0749-6419(01)00015-8.

Benzerga, A.A., 2008. An analysis of exhaustion hardening in micron-scale plasticity. Int. J. Plast. 24, 1128–1157. https://doi.org/10.1016/j.ijplas.2007.08.010.

Bertin, N., Tomé, C., Beyerlein, I., Barnett, M., Capolungo, L., 2014. On the strength of dislocation interactions and their effect on latent hardening in pure magnesium. Int. J. Plast. 62, 72–92. https://doi.org/10.1016/j.ijplas.2014.06.010.

Beyerlein, I.J., Tomé, C.N., 2007. Modeling transients in the mechanical response of copper due to strain path changes. Int. J. Plast. 23 (4), 640–664. https://doi.org/10.1016/j.ijplas.2006.08.001.

Bong, H.J., Barlat, F., Lee, M.-G., 2016. Probing formability improvement of ultra-thin ferritic stainless steel bipolar plate of PEMFC in non-conventional forming process. Metallurg. Mater. Trans. A 47 (8), 4160–4174. https://doi.org/10.1007/s11661-016-3561-0.

Brown, L.M., 1977. Orowan's explanation of the Bauschinger effect. Scr. Metall. 11 (2), 127–131. https://doi.org/10.1016/0036-9748(77)90291-5.

Caillard, D., Martin, J., 2003. Thermally Acticated Mechanisms in Crystal Plasticity. 8 Pergamonhttps://doi.org/10.1017/CBO9781107415324.004.

Campbell, J.D., Eleiche, A.M., Tsao, M.C.C., 1977. Strength of metals and alloys at high strains and strain rates. In: Jaffee, R.I., Wilcox, B.A. (Eds.), Fundamental Aspects of Structural Alloy Design. Springer US, Boston, MA, pp. 545–563. https://doi.org/10.1007/978-1-4684-2421-8_19.

Carvalho Resende, T., Bouvier, S., Abed-Meraim, F., Balan, T., Sablin, S.S., 2013. Dislocation-based model for the prediction of the behavior of b.c.c. materials - grain size and strain path effects. Int. J. Plast. 47, 29–48. https://doi.org/10.1016/j.ijplas.2013.01.003.

Diologent, F., Goodall, R., Mortensen, A., 2011. Activation volume in microcellular aluminium: size effects in thermally activated plastic flow. Acta Mater. 59 (18), 6869–6879. https://doi.org/10.1016/j.actamat.2011.07.021.

Dotsenko, V.I., 1979. Stress relaxation in crystals. Phys. Status Solidi B 11, 11–43.

Duhamel, C., Brechet, Y., Champion, Y., 2010. Activation volume and deviation from Cottrell Stokes law at small grain size. Int. J. Plast. 26 (5), 747–757. https://doi.org/10.1016/j.ijplas.2009.10.003.

Eipert, I., Sivaswamy, G., Bhattacharya, R., Amir, M., Blackwell, P., 2014. Improvement in ductility in commercially pure titanium alloys by stress relaxation at room temperature. Key Eng. Mater. 611–612 (April), 92–98. 10.4028/www.scientific.net/KEM.611-612.92

Estrin, Y., 1998. Dislocation theory based constitutive modelling: foundations and applications. J. Mater. Process. Technol. 80–81, 33–39. https://doi.org/10.1016/S0924-0136(98)00208-8.

Fan, X.G., Yang, H., 2011. Internal-state-variable based self-consistent constitutive modeling for hot working of two-phase titanium alloys coupling microstructure

evolution. Int. J. Plast. 27 (11), 1833–1852. https://doi.org/10.1016/j.ijplas.2011.05.008.
Guo, S., He, Y., Li, Z., Lei, J., Liu, D., 2018. Size and stress dependences in the tensile stress relaxation of thin copper wires at room temperature. Int. J. Plast. (September), 1–19. https://doi.org/10.1016/J.IJPLAS.2018.09.001.
Gupta, I., Li, J.C.M., 1970. Stress relaxation, internal stress, and work hardening in some bcc metals and alloys. Metallurg. Trans. 1, 2323–2330. https://doi.org/10.1007/BF02643451.
Ha, J., Lee, J., Kim, J.H., Lee, M.G., Barlat, F., 2017. Investigation of plastic strain rate under strain path changes in dual-phase steel using microstructure-based modeling. Int. J. Plast. 93, 89–111. https://doi.org/10.1016/j.ijplas.2017.02.005.
Hamelin, C.J., Diak, B.J., Pilkey, A.K., 2011. Multiscale modelling of the induced plastic anisotropy in bcc metals. Int. J. Plast. 27 (8), 1185–1202. https://doi.org/10.1016/j.ijplas.2011.01.003.
Hansen, B.L., Beyerlein, I.J., Bronkhorst, C.A., Cerreta, E.K., Dennis-Koller, D., 2013. A dislocation-based multi-rate single crystal plasticity model. Int. J. Plast. 44, 129–146. https://doi.org/10.1016/j.ijplas.2012.12.006.
Hariharan, K., Dubey, P., Jain, J., 2016. Time dependent ductility improvement of stainless steel SS 316 using stress relaxation. Mater. Sci. Eng. A 673, 250–256. https://doi.org/10.1016/j.msea.2016.07.074.
Hariharan, K., Kim, M.J., Hong, S.-T., Kim, D., Song, J.-H., Lee, M.-G., Han, H.N., 2017. Electroplastic behaviour in an aluminium alloy and dislocation density based modelling. Mater. Des. 124, 131–142. https://doi.org/10.1016/j.matdes.2017.03.072.
Hariharan, K., Majidi, O., Kim, C., Lee, M., Barlat, F., 2013. Stress relaxation and its effect on tensile deformation of steels. Mater. Des. 52, 284–288. https://doi.org/10.1016/j.matdes.2013.05.088.
Hart, E., 1970. A phenomenological theory for plastic deformation of polycrystalline metals. Acta Metall. 18, 599–610. https://doi.org/10.1016/0001-6160(70)90089-1.
Hu, J., Chen, B., Smith, D.J., Flewitt, P.E., Cocks, A.C., 2016. On the evaluation of the Bauschinger effect in an austenitic stainless steel-the role of multi-scale residual stresses. Int. J. Plast. 84, 203–223. https://doi.org/10.1016/j.ijplas.2016.05.009.
Jeong, Y., Barlat, F., Tomé, C.N., Wen, W., 2017. A comparative study between micro- and macro-mechanical constitutive models developed for complex loading scenarios. Int. J. Plast. 93, 212–228. https://doi.org/10.1016/j.ijplas.2016.07.015.
Jiang, M., Devincre, B., Monnet, G., 2018. Effects of the grain size and shape on the flow stress: a dislocation dynamics study. Int. J. Plast. https://doi.org/10.1016/J.IJPLAS.2018.09.008.
Johnston, W.G., Gilman, J.J., 1959. Dislocation velocities, dislocation densities, and plastic flow in lithium fluoride crystals. J. Appl. Phys. 30, 129–144. https://doi.org/10.1063/1.1735121.
Khan, A.S., Liu, J., 2016. A deformation mechanism based crystal plasticity model of ultrafine-grained/nanocrystalline FCC polycrystals. Int. J. Plast. 86, 56–69. https://doi.org/10.1016/j.ijplas.2016.08.001.
Kocks, U.F., Mecking, H., 2003. Physics and phenomenology of strain hardening: the FCC case. Prog. Mater. Sci. 48, 171–273. https://doi.org/10.1016/S0079-6425(02)00003-8.
Krempl, E., 2001. Relaxation behavior and modeling. Int. J. Plast. 17, 1419–1436. https://doi.org/10.1016/S0749-6419(00)00092-9.
Kreyca, J., Kozeschnik, E., 2018. State parameter-based constitutive modelling of stress strain curves in al-Mg solid solutions. Int. J. Plast. 103 (October 2017), 67–80. https://doi.org/10.1016/j.ijplas.2018.01.001.
Li, J.C., 2000. Charged dislocations and plasto-electric effect in ionic crystals. Mater. Sci. Eng. A 287, 265–271. https://doi.org/10.1016/S0921-5093(00)00784-X.
Li, J.C.M., Chau, C.C., 2006. Internal stresses in plasticity, microplasticity and ductile fracture. Mater. Sci. Eng., A 421, 103–108. https://doi.org/10.1016/j.msea.2005.10.008.
Li, X., Li, J., Ding, W., Zhao, S., Chen, J., 2017. Stress relaxation in tensile deformation of 304 stainless steel. J. Mater. Eng. Perform. 26 (2), 630–635. https://doi.org/10.1007/s11665-016-2496-3.
Lindgren, L.E., Hao, Q., Wedberg, D., 2017. Improved and simplified dislocation density based plasticity model for AISI 316 L. Mech. Mater. 108, 68–76. https://doi.org/10.1016/j.mechmat.2017.03.007.
Ma, Z., Zhan, L., Liu, C., Xu, L., Xu, Y., Ma, P., Li, J., 2018. Stress-level-dependency and bimodal precipitation behaviors during creep ageing of Al-Cu alloy: experiments and modeling. Int. J. Plast. 110 (July), 183–201. https://doi.org/10.1016/j.ijplas.2018.07.001.
Majidi, O., Barlat, F., Korkolis, Y.P., Fu, J., Lee, M.G., 2016. Thermal effects on the enhanced ductility in non-monotonic uniaxial tension of DP780 steel sheet. Met. Mater. Int. 22 (6), 968–973. https://doi.org/10.1007/s12540-016-6210-7.
Martin, J.L., Lo Piccolo, B., Kruml, T., Bonneville, J., 2002. Characterization of thermally activated dislocation mechanisms using transient tests. Mater. Sci. Eng., A 322, 118–125. https://doi.org/10.1016/S0921-5093(01)01124-8.
Mohebbi, M.S., Akbarzadeh, A., 2017. Development of equations for strain rate sensitivity of UFG aluminum as a function of strain rate. Int. J. Plast. 90, 167–176. https://doi.org/10.1016/J.IJPLAS.2017.01.003.
Mohebbi, M.S., Akbarzadeh, A., Yoon, Y.-O., Kim, S.-K., 2015. Stress relaxation and flow behavior of ultrafine grained AA 1050. Mech. Mater. 89, 23–34. https://doi.org/10.1016/j.mechmat.2015.06.001.
Muhammad, W., Brahme, A.P., Kang, J., Mishra, R.K., Inal, K., 2017. Experimental and numerical investigation of texture evolution and the effects of intragranular backstresses in aluminum alloys subjected to large strain cyclic deformation. Int. J. Plast. 93, 137–163. https://doi.org/10.1016/j.ijplas.2016.11.003.
Okazaki, K., Aono, Y., Kagawa, M., 1976. Mobile dislocations during stress relaxation in an Fe-0.056 at. % Ti alloy. Acta Metall. 24, 1121–1130.
Prasad, K., Krishnaswamy, H., Jain, J., 2018. Leveraging transient mechanical effects during stress relaxation for ductility improvement in aluminium AA 8011 alloy. J. Mater. Process. Technol. 255, 1–7.
Rauch, E.F., Gracio, J.J., Barlat, F., 2007. Work-hardening model for polycrystalline metals under strain reversal at large strains. Acta Mater. 55, 2939–2948. https://doi.org/10.1016/j.actamat.2007.01.003.
Rohde, R., Jones, W., Swearengen, J., 1981. Deformation modeling of aluminum: stress relaxation, transient behavior, and search for microstructural correlations. Acta Metall. 29, 41–52. https://doi.org/10.1016/0001-6160(81)90085-7.
Sargent, G., Jones, G., Conrad, H., 1969. Work hardening during stress relaxation in titanium at 300 degrees K. Scr. Metall. 3 (7), 481–484.
Sinha, N.K., 2003. Viscous and delayed-elastic deformation during primary creep-using strain relaxation and recovery test. Scr. Mater. 48, 1507–1512. https://doi.org/10.1016/S1359-6462(03)00016-2.
Spätig, P., Bonneville, J., Martin, J.-L., 1993. A new method for activation volume measurements: application to Ni3(Al,Hf). Mater. Sci. Eng. A 167, 73–79. https://doi.org/10.1016/0921-5093(93)90339-G.
Trojanová, Z., Máthis, K., Lukáč, P., Németh, G., Chmelík, F., 2011. Internal stress and thermally activated dislocation motion in an AZ63 magnesium alloy. Mater. Chem. Phys. 130, 1146–1150. https://doi.org/10.1016/j.matchemphys.2011.08.045.
Varma, A., Gokhale, A.R., Jain, J., Hariharan, K., Cizek, P., Barnett, M., 2018. Investigation of stress relaxation mechanisms for ductility improvement in SS316L. Philos. Mag. 98, 165–181. https://doi.org/10.1080/14786435.2017.1398422.
Wang, H., Capolungo, L., Clausen, B., Tomé, C.N., 2017. A crystal plasticity model based on transition state theory. Int. J. Plast. 93, 251–268. https://doi.org/10.1016/j.ijplas.2016.05.003.
Wang, H., Clausen, B., Capolungo, L., Beyerlein, I.J., Wang, J., Tomé, C.N., 2016a. Stress and strain relaxation in magnesium AZ31 rolled plate: in-situ neutron measurement and elastic viscoplastic polycrystal modeling. Int. J. Plast. 79, 275–292. https://doi.org/10.1016/j.ijplas.2015.07.004.
Wang, Y.Q., Spindler, M.W., Truman, C.E., Smith, D.J., 2016b. Critical analysis of the prediction of stress relaxation from forward creep of Type 316H austenitic stainless steel. Mater. Des. 95, 656–668. https://doi.org/10.1016/j.matdes.2016.01.118.
Xiao, L., Bai, J., 1998. Stress relaxation properties and microscopic deformation structure of H68 and QSn6.5–0.1 copper alloys at 353 K. Mater. Sci. Eng. A 244, 250–256. https://doi.org/10.1016/S0921-5093(97)00688-6.
Yang, F., Peng, L., Okazaki, K., 2006. Impression stress relaxation of Sn3.5Ag eutectic alloy. J. Mater. Res. 21 (December 2005), 2653–2659. https://doi.org/10.1557/jmr.2006.0335.
Zecevic, M., Knezevic, M., 2015. A dislocation density based elasto-plastic self-consistent model for the prediction of cyclic deformation: application to AA6022-T4. Int. J. Plast. 72, 200–217. https://doi.org/10.1016/j.ijplas.2015.05.018.
Zecevic, M., Knezevic, M., 2018. Latent hardening within the elasto-plastic self-consistent polycrystal homogenization to enable the prediction of anisotropy of AA6022-T4 sheets. Int. J. Plast. 105 (September 2017), 141–163. https://doi.org/10.1016/j.ijplas.2018.02.007.
Zheng, J.H., Lin, J., Lee, J., Pan, R., Li, C., Davies, C.M., 2018. A novel constitutive model for multi-step stress relaxation ageing of a pre-strained 7xxx series alloy. Int. J. Plast. 106 (February), 31–47. https://doi.org/10.1016/j.ijplas.2018.02.008.